Research in Astron. Astrophys. **2010** Vol. **10** No. **7**, 599–611
http://www.raa-journal.org *http://www.iop.org/journals/raa*

***R**esearch in*
***A**stronomy and*
***A**strophysics*

EDITOR'S RECOMMENDATION

New planetary nebulae in the outskirts of the Andromeda Galaxy discovered with the Guoshoujing Telescope (LAMOST)

Hai-Bo Yuan[1], Xiao-Wei Liu[1,2], Zhi-Ying Huo[1], Hui-Hua Zhang[1], Yong-Heng Zhao[3], Jian-Jun Chen[3], Zhong-Rui Bai[3], Hao-Tong Zhang[3], Hua-Wei Zhang[1], Ruben García-Benito[2], Mao-Sheng Xiang[4], Hong-Liang Yan[3], Juan-Juan Ren[3], Shi-Wei Sun[3], Yong Zhang[5], Ye-Ping Li[5], Qi-Shuai Lu[5], You Wang[5], Ji-Jun Ni[5] and Hai Wang[5]

[1] Department of Astronomy, Peking University, Beijing 100871, China; *x.liu@pku.edu.cn*
[2] Kavli Institute for Astronomy and Astrophysics, Peking University, Beijing 100871, China
[3] National Astronomical Observatories, Chinese Academy of Sciences, Beijing 100012, China
[4] Department of Astronomy, Beijing Normal University, Beijing 100875, China
[5] Nanjing Institute of Astronomical Optics & Technology, Chinese Academy of Sciences, Nanjing 210042, China

Received 2010 April 6; accepted 2010 May 20

Abstract Planetary nebulae (PNe) are good tracers of the stellar populations, chemical composition and dynamics of their host galaxies. This paper reports the discovery of new PNe in the outskirts of the Andromeda Galaxy (M 31) with the Guoshoujing Telescope (GSJT, formerly named the Large Sky Area Multi-Object Fiber Spectroscopic Telescope–LAMOST) during its early commissioning phase. In total, 36 candidates selected from SDSS photometry are confirmed in terms of their PN nature, including 17 new discoveries and another 19 previously known emission line objects. Their positions, spectra, radial velocities and m_{5007} magnitudes are presented. We discuss the potential for detecting more PNe in M 31 with GSJT's multi-object spectroscopy and the related applications in studies of the dynamics and chemistry of M 31 and its assemblage history.

Key words: galaxies: individual (M 31) — planetary nebulae: general

1 INTRODUCTION

China has recently completed construction of the Large Sky Area Multi-Object Fiber Spectroscopic Telescope (LAMOST; Wang et al. 1996; Su et al. 1998; Xing et al. 1998; Zhao 2000; Cui et al. 2004; Zhu et al. 2006; Cui et al. in preparation; c.f. *http://www.lamost.org/website/en/*), now named Guoshoujing Telescope (GSJT), which is an innovative quasi-meridian reflecting Schmidt telescope capable of simultaneously recording spectra of up to 4 000 objects with a field of view of 5 ° in diameter. The telescope, located at Xinglong Station and operated by the National Astronomical

Observatories, is currently undergoing commissioning, with major Galactic and extragalactic surveys expected to commence in late 2011.

Nine commissioning fields (hereafter Fields F01 to F09) have been selected and submitted to the GSJT operation center by the GSJT Galactic Working Group. The fields include two near the Andromeda Galaxy (M 31) – F03 centered close to the center of its optical disk and F02 toward the north-eastern outskirts of its halo. The two fields were proposed considering:

(1) M 31 is the largest galaxy of the Local Group and hosts a variety of interesting targets such as PNe, H II regions and globular clusters that are easily detectable with the GSJT. Kinematic and elemental abundance studies of those objects can shed light on the composition, dynamics and structure of M 31 and further aid in understanding the formation and evolution of galaxies;
(2) M 31 is easily accessible from the geodesic location of the GSJT during the best observational season (September to March). Being the nearest large (extragalactic) spiral galaxy, M 31 extends several degrees over the sky. Targeting M 31 utilizes the unique large field of view offered by the GSJT;
(3) The Sloan Digital Sky Survey (SDSS; York et al. 2000) has photometrically scanned the $ugriz$ bands in a large area of about $5^\circ \times 20^\circ$ around M 31 (runs 3366, 3367, 6426 and 7210) and obtained three spectroscopic plates (1468, 1471 and 1472), targeting low-redshift background quasars in two fields in the outskirts of M 31 (c.f. Adelman-McCarthy et al. 2006, 2007), thus providing plenty of spectra for comparison with GSJT observations. The accurate SDSS photometry can also be utilized to select interesting targets such as PN candidates, the topic of the current work.

A variety of targets were selected for Fields F02 and F03, including normal and luminous red galaxies, low-redshift quasars and spectroscopic standard stars (F sub-dwarfs), selected from the SDSS photometry, as well as stars selected from the Two Micron All Sky Survey (Skrutskie et al. 2006). Also included in Field 03 are PNe and PN candidates. PNe in M 31 are readily detectable with the GSJT and their prominent narrow emission line spectra can be utilized to characterize the performance of the GSJT, such as the overall instrumental throughput, the precision of fiber positioning, the spectral resolutions, and the accuracy of wavelength calibration and radial velocity determinations. PNe are also good tracers of the populations of low- to intermediate-mass stars, and are widely used to probe the kinematic structures (e.g. Hui et al. 1995; Arnaboldi et al. 1996; Méndez et al. 2001; Peng et al. 2004) and the chemical enrichment history (e.g. Jacoby & Ciardullo 1999; Bresolin et al. 2010) of the host galaxies. Intracluster PNe are used to study the intracluster stellar populations and to probe the gravitational potential of clusters of galaxies (Theuns & Warren 1997; Feldmeier et al. 1998; Mihos et al. 2009). PNe have even been used as standard candles to measure the distances to the host galaxies and determine the Hubble constant (Ford & Jenner 1979; Jacoby 1989; Ciardullo et al. 1989).

Many efforts have been carried out to identify and study PNe in M 31. Using a plate-filter combination technique to isolate the [O III]λ5007 emission line, Nolthenius & Ford (1987) found 34 PNe and used them to probe the dynamics of the outer disk and bulge of M 31. Ciardullo et al. (1989) identified 429 PN candidates by comparing the [O III]λ5007 narrow band and adjacent continuum medium band images in an irregularly shaped area of approximately $33' \times 3'$ in the disk of M 31. Meyssonnier et al. (1993) surveyed nearly the whole extent of M 31 using an objective-prism and found 1515 emission line objects, including candidates of PNe, Wolf-Rayet stars, H II regions, emission line galaxies and quasars. Hurley-Keller et al. (2004, hereafter HK04) identified 135 PNe in the southwest quadrant of M 31's outer bulge/halo with narrow-band filters and followup spectroscopy. The kinematics of these PNe suggests that M 31 has a much larger extended bulge than the Milky Way. Kniazev et al. (2005, hereafter K05) selected 130 PN candidates based on their SDSS magnitudes and colors. They obtained spectra for 85 of them, among which 70 were confirmed as PNe. Halliday et al. (2006, hereafter H06) measured radial velocities for a sample of 723 PNe in the disk

and bulge of M 31 with a wide-field multi-object spectrograph and used the data to constrain the mass distribution and velocity anisotropy of the disk, bulge and halo of M 31. In the most comprehensive and thorough of all, Merrett et al. (2006, hereafter M06) surveyed the M 31 field out to a radius of 1.5° using the Planetary Nebula Spectrograph, an innovative instrument capable of simultaneously identifying PNe and measuring their radial velocities. Additional data were also obtained for selected areas extending to larger radii along the major and minor axes, and around regions of the Northern Spur and Southern Stream (Ibata et al. 2001). They obtained positions, magnitudes and velocities for 3300 emission-line objects, of which 2730 are probably PNe. M06 used this, hitherto the largest sample of PNe ever assembled for an external galaxy, to constrain the dynamics of M 31 and its PN population.

In this paper, we report the discoveries of new PNe using the early GSJT commissioning data in a field of view of about 5° near the center of M 31, with candidates selected from SDSS photometry based on the algorithm of K05, which is revised to increase the completeness (at the cost of reducing the efficiency). We describe the target selection, observation and data reduction in Section 2, and present the results and discussion in Section 3.

2 TARGET SELECTION, OBSERVATION AND DATA REDUCTION

K05's selection criteria were based on a test sample of 30 known PNe that have SDSS photometry in the u, g, r and i bands. Applying the criteria to the whole M 31 area scanned by SDSS yields 162 PN candidates, including the 30 genuine PNe of the test sample. Since then, a lot more PNe have been discovered, especially by the Planetary Nebula Spectrograph survey carried out by M06. We have combined the samples of known PNe from M06, H06 and HK04 and cross-identified them with the SDSS photometric catalogs of the M 31 stripes, using a matching radius of $1''$, $1''$ and $3''$ for the samples of HK04, H06 and M06, respectively. This yields a test sample of 180 genuine PNe with the SDSS u, g, r and i-band photometry[1]. Note that the SDSS criteria for star-galaxy separation work well at a reliability level better than 90% up to $r = 21.6$, but worsen at fainter magnitudes (Abazajian et al. 2003). Thus in addition to point sources brighter than $r = 21.5$ (at the distance of M 31, 785 kpc given by McConnachie et al. 2005, all PNe appear as point-sources), all SDSS sources, point or extended, were included in the current analysis, as in K05. From this much expanded test sample, we find that, although the algorithm developed by K05 has a very high success rate (82 per cent), applying it to the test sample yields only 50 candidates. In other words, 70 per cent of the genuine PNe have been left out. This is not surprising. PNe span a wide range of excitation classes and metallicities, and emit spectra of vastly different relative line strengths, leading to a wide spread in the SDSS color-color diagrams. Broad band photometry is after all not particularly suitable to select emission line objects such as PNe. With 4 000 fibers available from the GSJT, we can afford to loose the PN selection criteria to increase the completeness, at the cost of, unavoidably, lowering the efficiency. We have adopted the criteria: $u - g > 0.5$, $g - r < -0.3$, $r - i < 0.4$, $21 < r < 23.5$, and $g > 20.5$. Here all magnitudes are psf magnitudes. Applying these criteria to the test sample of 180 PNe yields 68 PN candidates, representing a 10 per cent increase in completeness compared to

[1] Approaching the bright disk of M 31 where most PNe are concentrated, the SDSS source catalogs of individual fields, available from the SDSS Data Archive Server (*http://das.sdss.org/www/html/*), are either incomplete or contain no sources at all due to extreme field crowdedness. This, together with the fact that the SDSS, a broad band survey with a limiting magnitude of 22.2 in the g and i bands, is deep enough to detect only the brightest PNe in M 31, explains the small number of PNe cross-identified in the SDSS dataset. Finally, we note that a comparison of the SDSS photometric data of M 31 with those obtained in the Xuyi Digital Sky Survey of the Galactic Anti-center (XDSS-GAC), an ongoing program led by XWL to survey a sky area of over 6 000 square degrees centered on the Galactic anticenter in the SDSS g, r and i bands with the Xuyi 1.0/1.2 m Schmidt Telescope of the Purple Mountain Observatory, shows that there are systematic errors in the photometric zero points of individual SDSS fields of M 31, at the level of a few per cent. Such systematics are not present in the SDSS data of the northern Galactic Cap that overlap with our data. The XDSS-GAC reaches a limiting magnitude fainter than 19 and will be used to select input targets for a forthcoming large GSJT spectroscopic survey of several million stars toward the Galactic anticenter.

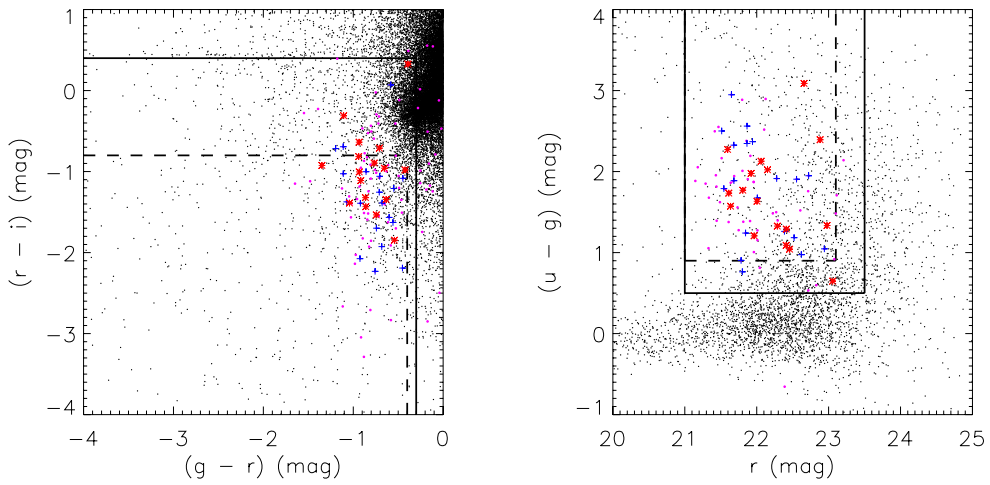

Fig. 1 *Left panel:* $r-i$ versus $g-r$ color-color diagram for SDSS sources of the M 31 stripes; *Right panel:* $u-g$ versus r color-magnitude diagram of the same set of data *after* applying the color cuts shown in the left panel. In both panels, dashed lines represent the color and magnitude cuts adopted by K05, whereas solid lines denote our less stringent criteria for PN candidates. Purple dots are known PNe from the test sample. Objects newly discovered as PNe and confirmed in terms of their PN nature are marked by red stars and blue crosses, respectively.

the criteria of K05. We then apply the algorithm to the whole area of M 31 scanned by the SDSS. This yields 1070 candidates (see Figs. 1 and 2). Note that most of our candidates are well outside the disk, so contamination from H II regions, which exhibit emission line spectra similar to PNe but are confined to spiral arms in the disk, is likely to be small.

The F03 field was observed on 2009 October 19 and December 15. On each occasion, two 1800 s exposures were obtained. Arc and twilight-sky/dome flat exposures were taken for wavelength calibration and flat-fielding, respectively. The low spectral resolution mode of $R = 1\,000$ was used on October 19, whereas the higher resolution mode of $R = 2\,000$ was used on December 15 by inserting slit masks of 1.65″ wide, half the fiber diameter of 3.30″. The $R = 2\,000$ mode was thus achieved at the cost of losing 39 per cent of the incoming light from the geometric consideration alone. Extra loss of light may occur if the fibers are not perfectly aligned with the slit masks. Given that PN emission lines are narrow (typical expansion velocities $\lesssim 30\,\mathrm{km\,s^{-1}}$) and unresolved, their detections and radial velocity measurements benefit from the employment of the $R = 2\,000$ mode by increasing the line to continuum (sky and nebular/stellar) contrasts.

The data were reduced with the standard procedures using the GSJT 2D pipeline (Luo et al. 2004), including steps of bias subtraction, cosmic-ray removal, 1D spectral extraction, flat-fielding, wavelength calibration, and sky subtraction. Flux calibration was not reliable, and thus was not performed. Spectra from some CCDs (more often of the red arms) could not be reduced because of the presence of electromagnetic interference or very high levels of dark current.

To test the accuracy of wavelength calibration, we compared the observed wavelengths of the strong sky emission lines [O I]λ5577 and λ6300 recorded in the blue and red arms, respectively, for the $R = 2\,000$ mode data obtained in 2009 December. Although there were systematic variations from spectrograph to spectrograph, the errors were typically smaller than $8\,\mathrm{km\,s^{-1}}$, except for some rare cases where uncertainties up to $15\,\mathrm{km\,s^{-1}}$ were observed.

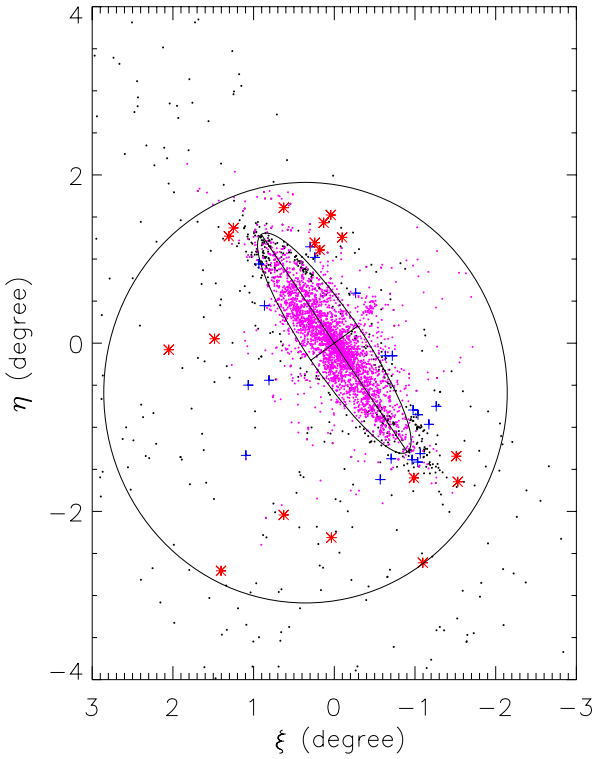

Fig. 2 Spatial distribution of previously known emission line objects in the field of M 31 (*purple dots*), PN candidates selected from the SDSS M 31 photometric data (*black dots*) and GSJT newly discovered (*red stars*) or confirmed (*blue crosses*) PNe. The coordinates ξ and η represent an M 31-based reference frame defined by Huchra et al. (1991), $\xi = \sin$ (RA - RA_0) cos (Dec) and $\eta = \sin(\mathrm{Dec})\cos(\mathrm{Dec}_0) - \cos(\mathrm{RA}-\mathrm{RA}_0)\cos(\mathrm{Dec})\sin(\mathrm{Dec}_0)$, where $\mathrm{RA}_0 = 00^{\mathrm{h}}42^{\mathrm{m}}44\overset{\mathrm{s}}{.}4$, $\mathrm{Dec}_0 = 41^\circ16'08''$ (J2000.0) is the optical center of M 31 (de Vaucouleurs et al. 1991). The inner ellipse represents the optical disk of M 31, assuming a radius $R_{25} = 95.3'$ (de Vaucouleurs et al. 1991), an inclination angle $i = 77^\circ$ and a position angle PA = 35° (Walterbos & Kennicutt 1987). The two orthogonal lines denote the galaxy's major and minor axes. The big circle delineates the 5° GSJT field of view for test field F03, centered at $\mathrm{RA} = 00^{\mathrm{h}}44^{\mathrm{m}}37\overset{\mathrm{s}}{.}2$, $\mathrm{Dec.} = +40^\circ40'45''$ (J2000.0).

3 RESULTS AND DISCUSSION

Spectra of PN candidates were visually examined one by one. In total, 199 candidates were observed on 2009 December 15 and 38 were confirmed as PNe and 1 as an H II region. Of the 38 newly confirmed PNe, queries of the SIMBAD Astronomical Database show that 16 are new discoveries, 17 are previously known emission line object candidates, and the remaining 5 are previously known PNe. On 2009 October 19, 197 PN candidates were observed, among which 33 were confirmed as PNe and 2 as H II regions. Among the 33 objects, 13 are newly identified PNe, 15 are previously known emission line objects but are now confirmed in terms of their PN nature, and the last 5 are known PNe. There was a significant overlap among objects observed in October and December. Combining results from the two nights yields 17 newly discovered PNe (c.f. Table 1 and Figs. 3 and 4) and 19 newly confirmed PNe (c.f. Table 2 and Figs. 5 and 6).

Table 1 New Planetary Nebulae Discovered with the GSJT in Commissioning Field F03

Object[a]	SDSS photometry $ugriz$ mags					RA (J2000.0)	Dec (J2000.0)	Fiber-ID[b]	$v_{\rm helio}$ (km s^{-1})	m_{5007}
J004255.34+385726.3	23.07	22.42	23.06	24.40	23.01	10.730587	38.957298	01–03–18	–497	23.0
J003707.12+383856.9	22.57	21.48	22.41	23.41	21.90	9.2796779	38.649138	02–09–18	–273	21.1
J004558.51+391325.4	23.19	21.86	22.29	23.27	23.79	11.493811	39.223730	05–01–20	–309	21.1
J004955.17+383249.0	22.79	21.75	22.46	23.17	22.66	12.479859	38.546954	07–10–20	–362	21.9
J005038.67+411815.9	22.86	20.88	21.92	23.31	22.38	12.661130	41.304424	09–08–21	–187	21.7
J003447.57+393612.2	22.35	20.78	21.64	23.07	22.88	8.6982158	39.603386	10–02–11	–470	21.8
J003451.20+395429.0	22.60	20.87	21.61	23.15	22.39	8.7133230	39.908051	10–03–21	–486	21.6
J003736.57+393935.6	23.93	21.53	22.88	23.81	23.10	9.4023708	39.659894	10–07–21	–442	21.4
J004212.44+423134.2	23.20	21.87	22.98	23.29	23.09	10.551848	42.526170	11–01–03	–285	22.7
J004258.47+424732.6	22.63	21.42	21.96	23.81	22.81	10.743630	42.792389	11–01–04	–145	22.5
J004327.24+424203.5	22.77	21.48	22.41	23.05	21.94	10.863486	42.700965	11–01–15	–154	24.1
J004342.52+422235.5	23.25	21.12	22.06	22.88	22.18	10.927152	42.376529	11–04–13	–224	23.7
J004609.59+425238.7[c]	25.35	22.27	22.66	22.33	22.37	11.539952	42.877423	11–05–05	–19.5	23.6
J004949.82+423139.6[d]	23.52	21.50	22.15	23.11	22.37	12.457573	42.527661	12–03–03	–381	22.6
J004931.94+423737.9	22.81	21.04	21.81	22.70	23.56	12.383071	42.627192	12–03–24	–146	21.5
J005338.57+410932.3	22.72	21.09	22.00	23.11	23.76	13.410707	41.158980	13–06–13	–437	22.0
J004403.11+422746.6[e]	23.00	20.73	21.60	22.92	21.75	11.012974	42.462949	11–04–19	–234	20.1

[a] In format Jhhmmss.ss+ddmmss.s, where hhmmss.ss is the RA and ddmmss.s the Dec. of epoch J2000.0;

[b] In format ii-jj-kk, where ii is the spectrograph number (01–16), jj the fiber clip number (01–10) and kk the fiber number within the clip (01–25);

[c] Possibly associated with the Northern Spur (Ibata et al. 2001);

[d] Possibly associated with the extension of the Giant Stream (Merrett et al. 2003);

[e] Detected in the $R = 1\,000$ mode only.

For the 36 new PNe, we measured the observed wavelengths and recorded photon counts of the [O III]λ5007 line by gaussian profile fitting and calculated the heliocentric radial velocities. The net throughput, including the atmospheric effects of GSJT, was also derived by comparing the measured counts with the m_{5007} magnitudes given in M06. Typical values of the throughput were 1 per cent, but varied by a factor of two or more from fiber to fiber and from spectrograph to spectrograph. To deduce the m_{5007} magnitudes for the 36 newly discovered and confirmed PNe, we have assumed a uniform throughput of 1 per cent for all fibers. Magnitudes thus derived are tabulated in Tables 1 and 2, and are expected to be accurate to 0.6 mag. As a check, among the 180 known PNe in the test sample discussed in Section 2, 101 have m_{5007} measurements from the literature that are brighter than 23, and we find that for this sub-group of PNe there is a good linear relation between m_{5007} and the SDSS g-band magnitude: $m_{5007} = 1.15 \times g - (3.1 \pm 0.2)$. Applying this empirical relation to the 36 new PNe yields m_{5007} magnitudes that are consistent with the rough values estimated above assuming a constant 1 per cent throughput for the GSJT.

To estimate the accuracy of radial velocity measurements, we compared the GSJT results with those of H06 for 30 common objects and with M06 for more than 100 common objects. The typical uncertainties of H06 and M06 velocities used here are 5 km s^{-1} and 17 km s^{-1}, respectively. For the $R = 2\,000$ mode, the differences between the GSJT and the H06 velocities have an average value of -5 km s^{-1} (i.e. the GSJT velocities are slightly blue-shifted relative to the H06 value on average), with a standard deviation of 5 km s^{-1}. For the M06 sample, the corresponding values are $+3$ km s^{-1} and 21 km s^{-1}, respectively. For the $R = 1\,000$ mode, we find an average difference and standard deviation of -4 km s^{-1}($+10$ km s^{-1}) and 8 km s^{-1} (20 km s^{-1}), respectively, between the GSJT and H06 (M06) velocities. Thus, we estimate that GSJT radial velocities are accurate to within 5 and 10 km s^{-1} for the $R = 2\,000$ and 1 000 modes, respectively.

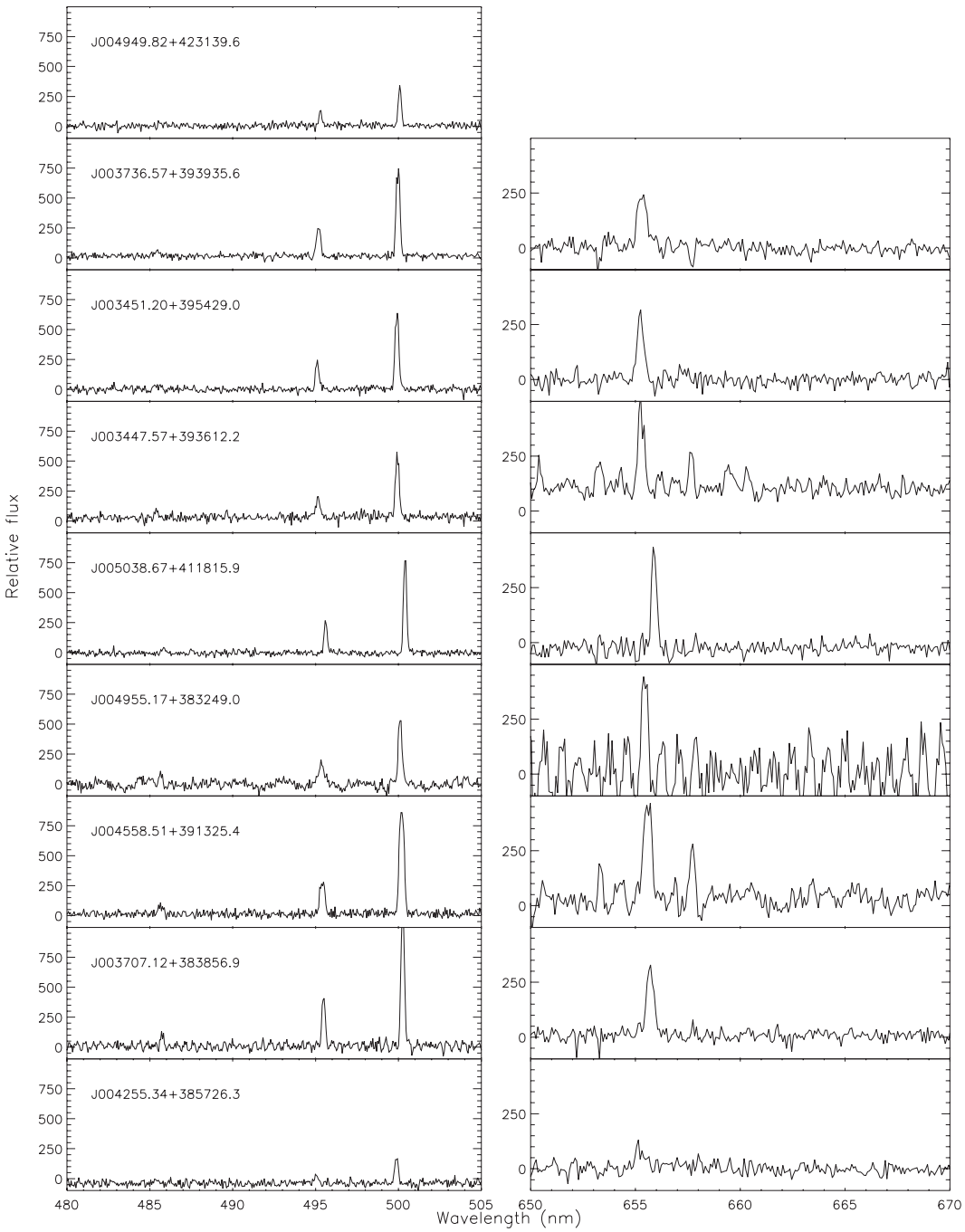

Fig. 3 Co-added GSJT spectra of newly discovered PNe observed on 2009 December 15 in $R = 2\,000$ mode. The relative fluxes are in units of counts per pixel.

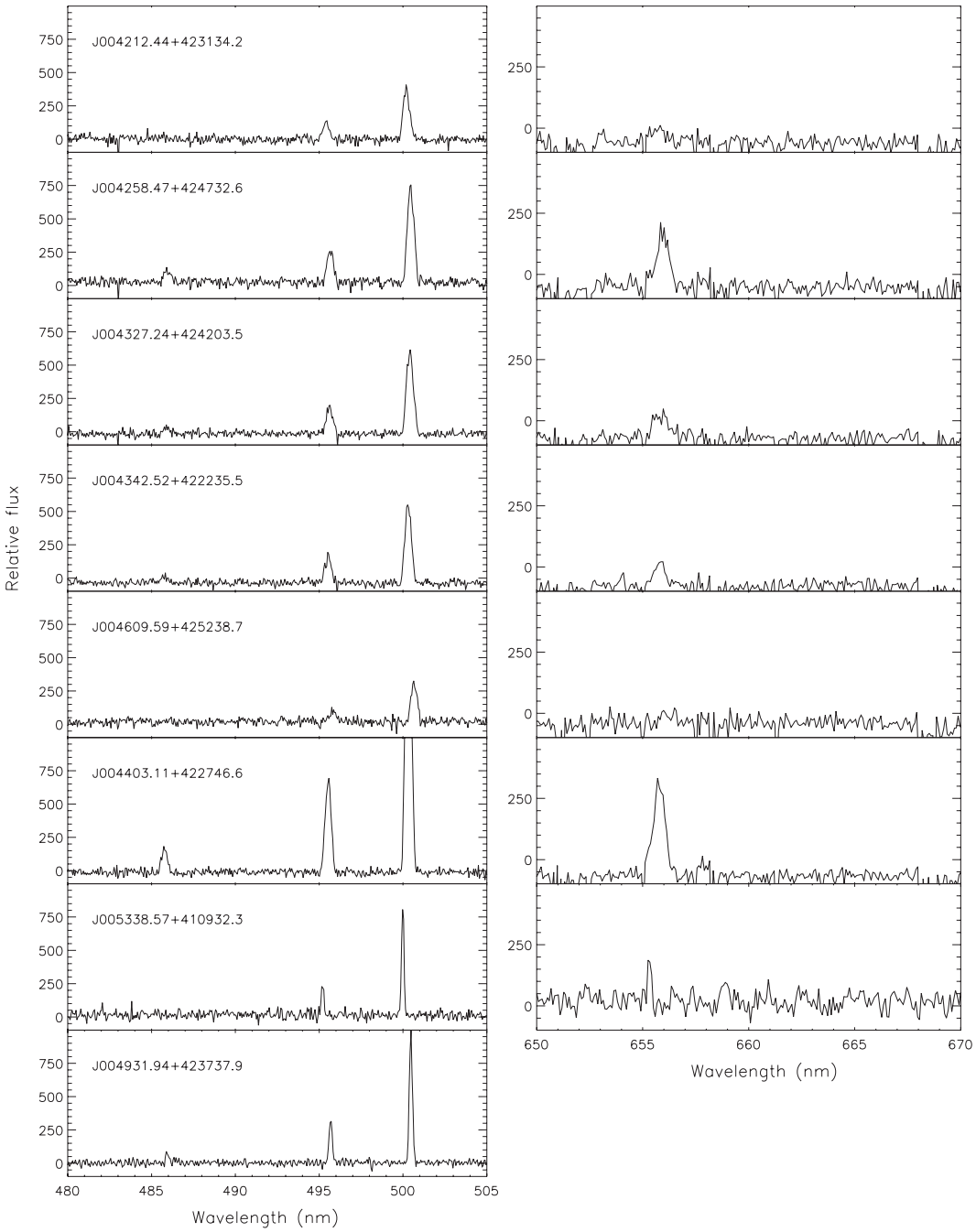

Fig. 4 Co-added GSJT spectra of newly discovered PNe observed on 2009 October 19 in $R = 1\,000$ mode except for J005338.57+410932.3 and J004931.94+423737.9, whose spectra were taken on 2009 December 15 in $R = 2\,000$ mode. The relative fluxes are in units of counts per pixel.

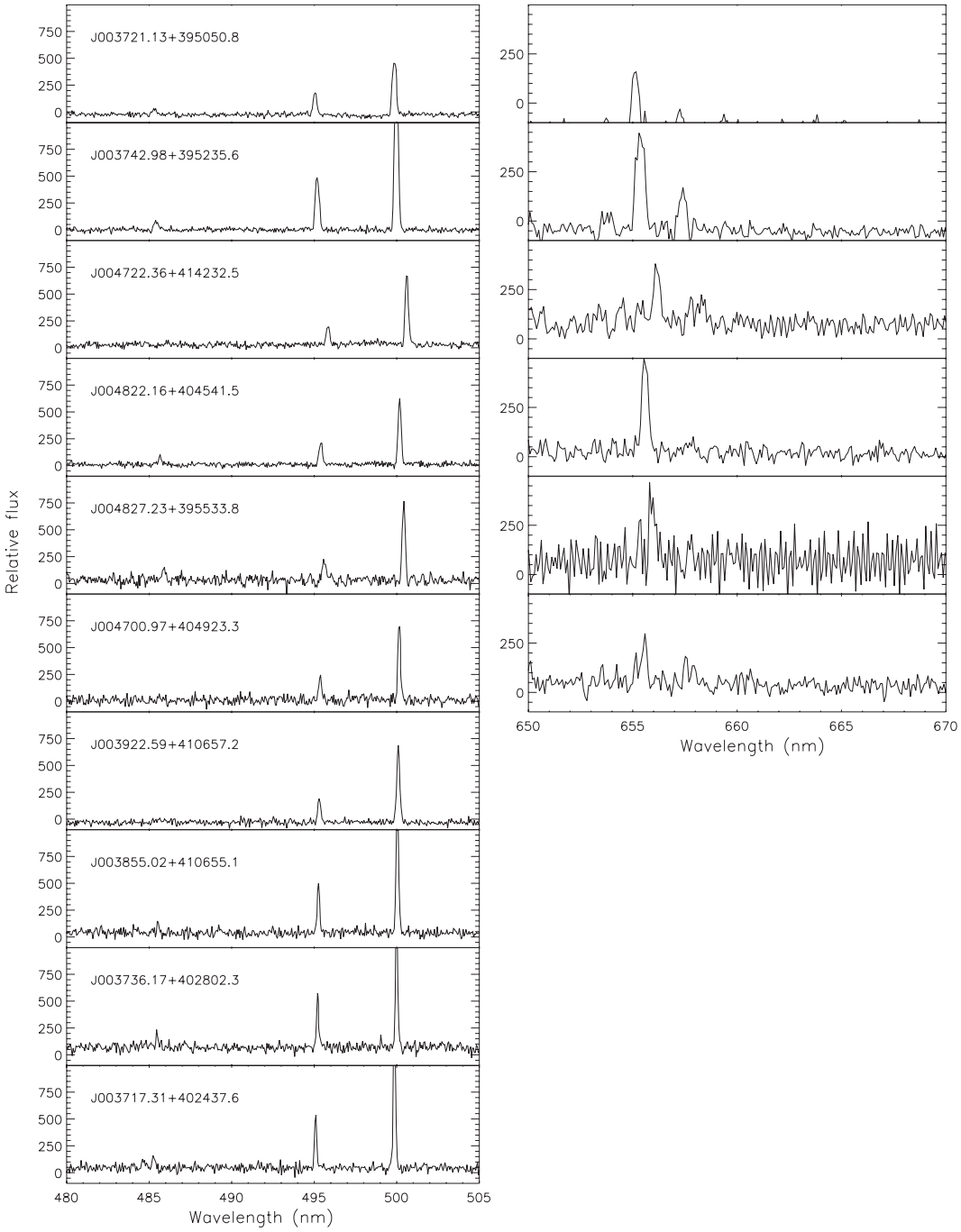

Fig. 5 Co-added GSJT spectra of newly confirmed PNe observed on 2009 December 15 in $R = 2\,000$ mode. The relative fluxes are in units of counts per pixel.

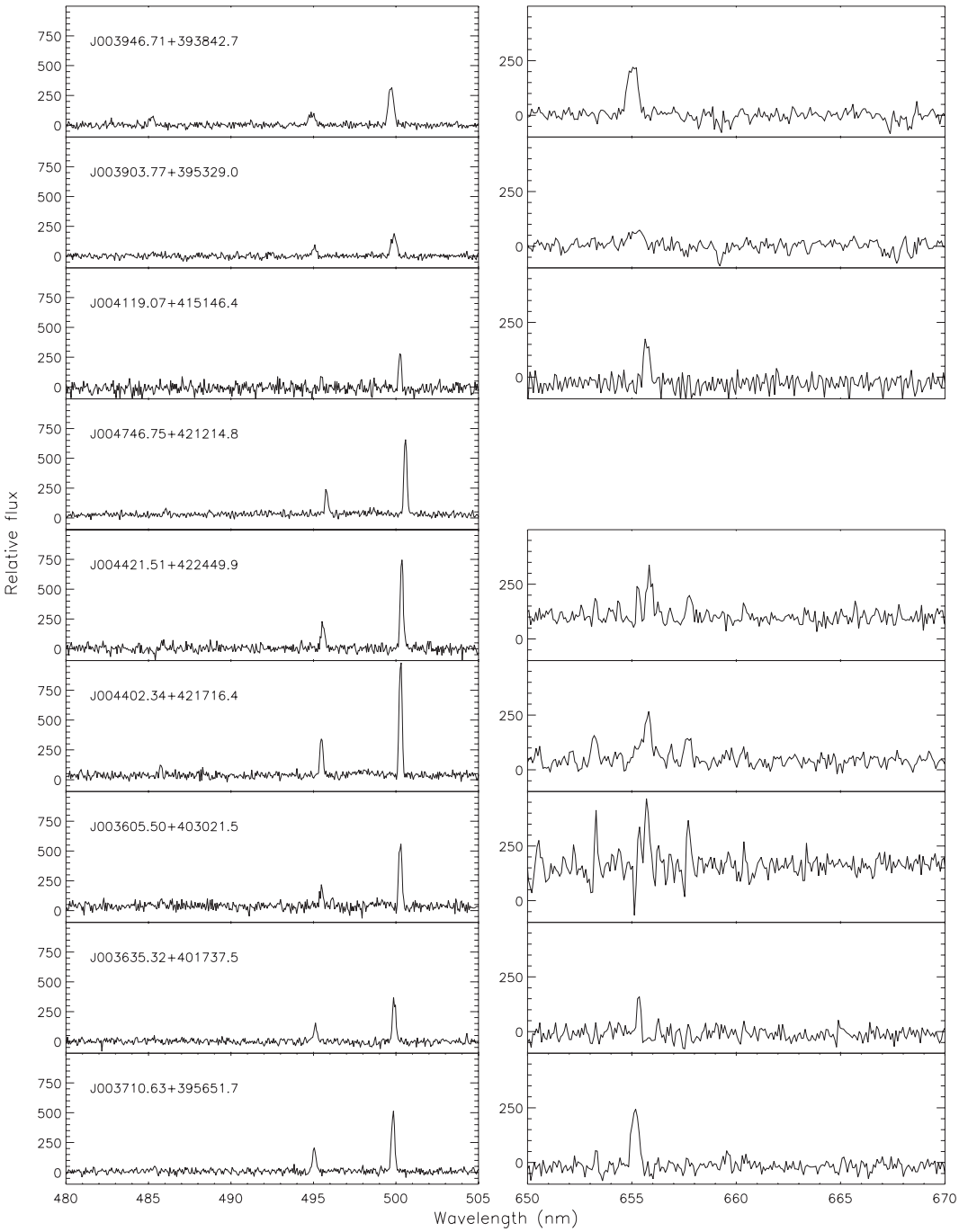

Fig. 6 Co-added GSJT spectra of newly confirmed PNe observed on 2009 December 15 in $R = 2\,000$ mode, except for J003903.77+395329.0 and J003946.71+393842.7, whose spectra were taken on 2009 October 19 in $R = 1\,000$ mode. The relative fluxes are in units of counts per pixel.

Table 2 Emission Line Objects Newly Confirmed in terms of their PN Nature by the GSJT Spectroscopy in Field F03

Object[a]	SDSS photometry $ugriz$ mags					RA (J2000.0)	Dec (J2000.0)	Fiber-ID[b]	$v_{\rm helio}$ (km s^{-1})	m_{5007}	Comment
J003717.31+402437.6	23.46	20.96	21.51	22.72	22.73	9.3221417	40.410457	03–04–06	–512	21.1	MLA 30
J003736.17+402802.3	22.77	20.99	21.54	23.17	21.99	9.4006892	40.467293	03–04–09	–433	21.3	MLA 35
J003855.02+410655.1	23.20	20.83	21.94	22.64	22.42	9.7292598	41.115297	03–06–00	–406	21.2	MLA 74
J003922.59+410657.2	23.68	20.73	21.65	23.04	23.31	9.8441195	41.115895	03–09–04	–373	21.8	MLA 105
J004700.97+404923.3	23.70	21.80	22.55	24.79	21.76	11.754060	40.823126	04–10–08	–340	22.1	HKPN M 31 131[e]
J004827.23+395533.8	22.24	21.33	21.78	22.87	22.58	12.113438	39.926066	08–01–06	–174	21.9	HKPN M 31 134
J004822.16+404541.5	22.48	21.24	21.84	23.41	23.08	12.092323	40.761535	09–01–14	–322	22.0	HKPN M 31 132
J004722.36+414232.5	23.29	20.94	21.86	23.94	22.68	11.843157	41.709021	09–05–06	–63	22.0	MLA 1292
J003742.98+395235.6	23.72	21.16	21.87	22.92	22.02	9.4290907	39.876568	10–07–01	–439	20.6	Ford M 31 335
J003721.13+395050.8	22.86	20.97	21.68	22.94	22.34	9.3380230	39.847448	10–07–17	–517	21.7	Ford M 31 337
J003710.63+395651.7	23.12	21.94	22.52	22.45	22.93	9.2942732	39.947684	10–09–06	–531	21.9	MLA 28
J003635.32+401737.5	22.85	21.88	22.62	24.32	23.89	9.1471587	40.293753	10–09–21	–490	22.4	MLA 15
J003605.50+403021.5	22.96	21.70	22.39	24.31	22.39	9.0229013	40.505966	10–10–19	–270	21.9	Ford M 31 360
J004402.34+421716.4	23.15	20.82	21.68	22.68	22.77	11.009767	42.287879	11–04–01	–256	21.5	MLA 904
J004421.51+422449.9	23.12	21.20	22.28	23.65	21.99	11.089636	42.413865	11–10–15	–216	21.8	MLA 972
J004746.75+421214.8	22.49	20.81	22.01	22.72	22.72	11.944776	42.204123	12–06–18	–84	22.0	MLA 1304
J004119.07+415146.4[c]	23.31	22.26	22.94	24.33	23.51	10.329479	41.862879	15–04–22	–279	22.8	NGC 205 69
J003903.77+395329.0[d]	23.56	21.61	22.72	23.75	23.08	9.7657020	39.891397	05–08–16	–502	22.9	HKPN M 31 7
J003946.71+393842.7[d]	22.11	21.35	21.80	23.99	22.05	9.9446212	39.645186	05–10–06	–607	22.2	HKPN M 31 31

[a] In format Jhhmmss.ss+ddmmss.s, where hhmmss.ss is the RA and ddmmss.s the Dec. of epoch J2000.0;

[b] In format ii-jj-kk, where ii is the spectrograph number (01–16), jj the fiber clip number (01–10) and kk the fiber number within the clip (01–25);

[c] Possibly associated with NGC 205 (Corradi et al. 2005);

[d] Detected in the $R = 1\,000$ mode only;

[e] Also see name MLA128.

Among the 36 newly discovered and confirmed PNe, 9 would be missed by the selection algorithm of K05. Our less stringent criteria increase the number of PN detections by 30 per cent, consistent with the expectations based on the test sample. It is almost impossible to estimate the efficiency of PN detection for the current work, given the uneven and far from optimized performance of the GSJT, not to mention malfunctions in some of the spectrographs. Based on the efficiency and completeness of K05, we estimate that there are a total of approximately 500 PNe among the sources in the M 31 field that are detected by the SDSS in the u, g, r, and i bands. Our criteria should lead to the discovery of 190 of them, of which 68 have already been found by previous surveys. Thus, among the 1070 PN candidates, 122 are expected to be genuine PNe. In other words, the efficiency of our algorithm is approximately 20 per cent.

In hierarchical cosmological models, the continual accretion of smaller galaxies contributes significantly to the growth of a larger galaxy, especially in its late evolutionary stage. The tidal disruption of these small systems is expected to result in loosely bound stars surrounding the galaxy, at distances up to 10–100 times the radius of the central disk. In the case of M 31, a large number of coherent stellar substructures have been detected in its outskirts (c.f. the most recent work by Ibata et al. 2007 and McConnachie et al. 2009). The number, luminosity, morphology and stellar population of the relics of this process provide important clues to the mass assemblage history of the galaxy. A comprehensive survey of these relics is, however, quite difficult given their intrinsic faintness and the vast space over which they are spread. PNe are easily detectable at the distance of M 31 for a GSJT class telescope given their bright narrow emission line spectra, and thus can serve as excellent tracers to study the chemistry, kinematics and stellar content of those substruc-

tures. As shown in Figure 2, all our newly discovered PNe are located well beyond the optical disk of M 31. The two outermost PNe, J003707.12+383856.9 and J004255.34+385726.3, have projected distances of 41.5 and 38.5 kpc, respectively, from the center of M 31 (assuming a distance of 785 kpc to M 31; McConnachie et al. 2005). In addition, based on its spatial position and radial velocity, J004949.82+423139.6 is possibly associated with an extension of the Southern Stream (Merrett et al. 2003). Similarly, J004609.59+425238.7 is possibly associated with the Northern Spur (Ibata et al. 2001) and J004119.07+415146.4 possibly with NGC 205, a satellite galaxy of M 31. Deep spectroscopic followup studies of the chemistry and kinematics of those far out nebulae or nebulae possibly associated with known substructures will be extremely interesting.

As the performance of the GSJT continues to improve, we plan to survey the whole SDSS area around M 31 and expect additional PNe to be discovered. The GSJT will also be a formidable facility to study the generated radial velocities of PNe in M 31, reducing their uncertainties (currently at the level of $\sim 15\,\mathrm{km\ s^{-1}}$ for the majority of them; M06) by a factor of two. A large sample of about 3 000 PNe with accurate radial velocity values will be an invaluable asset to study the kinematics of M 31 and its associated substructures.

Acknowledgements The Guoshoujing Telescope (GSJT) is a National Major Scientific Project built by the Chinese Academy of Sciences. Funding for the project has been provided by the National Development and Reform Commission. The GSJT is operated and managed by the National Astronomical Observatories, Chinese Academy of Sciences. This work has made use of the Sloan Digital Sky Survey (SDSS), the NASA/IPAC Extragalactic Database (NED) and the SIMBAD database.

References

Abazajian, K., et al. 2003, AJ, 126, 2081
Adelman-McCarthy, J. K., et al. 2006, ApJS, 162, 38
Adelman-McCarthy, J. K., et al. 2007, ApJS, 172, 634
Arnaboldi, M., Freeman, K. C., Mendez, R. H., et al. 1996, ApJ, 472, 145
Bresolin, F., Stasińska, G., Vílchez, J. M., Simon, J. D., & Rosolowsky, E. 2010, MNRAS, 372
Ciardullo, R., Jacoby, G. H., Ford, H. C., & Neill, J. D. 1989, ApJ, 339, 53
Corradi, R. L. M., Magrini, L., Greimel, R., et al. 2005, A&A, 431, 555
Cui, X., et al. 2004, Proc. SPIE, 5489, 974
de Vaucouleurs, G., de Vaucouleurs, A., Corwin, H. G., Jr., Buta, R. J., Paturel, G., & Fouqué, P. 1991, Third Reference Catalogue of Bright Galaxies (New York: Springer)
Feldmeier, J. J., Ciardullo, R., & Jacoby, G. H. 1998, ApJ, 503, 109
Ford, H. C., & Jenner, D. C. 1979, Bull. AAS, 10, 665
Halliday, C., Carter, D., Bridges, T. J., et al. 2006, MNRAS, 369, 97
Huchra, J. P., Brodie, J. P., & Kent, S. M. 1991, ApJ, 370, 495
Hui, X., Ford, H. C., Freeman, K. C., & Dopita, M. A. 1995, ApJ, 449, 592
Hurley-Keller, D., Morrison, H. L., Harding, P., & Jacoby, G. H. 2004, ApJ, 616, 804
Ibata, R., Irwin, M., Lewis, G., Ferguson, A. M. N., & Tanvir, N. 2001, Nature, 412, 49
Ibata, R., Martin, N. F., Irwin, M., Chapman, S., Ferguson, A. M. N., Lewis, G. F., & McConnachie, A. W. 2007, ApJ, 671, 1591
Jacoby, G. H., & Ciardullo, R. 1999, ApJ, 515, 169
Jacoby, G. H., Ciardullo, R., Booth, J., & Ford, H. C. 1989, ApJ, 344, 704
Jacoby, G. H., & Ford, H. C. 1986, ApJ, 304, 490
Kniazev, A. Y., Grebel, E. K., Zucker, D. B., Bell, E. F., Rix, H.-W., Martínez-Delgado, D., & Harris, H. C. 2005, Planetary Nebulae as Astronomical Tools, 804, 15

Luo, A.-L., Zhang, Y.-X., & Zhao, Y.-H. 2004, Proc. SPIE, 5496, 756
McConnachie, A. W., Irwin, M. J., Ferguson, A. M. N., Ibata, R. A., Lewis, G. F., & Tanvir, N. 2005, MNRAS, 356, 979
McConnachie, A. W., Irwin, M. J., Ibata, R. A., et al. 2009, Nature, 461, 66
Méndez, R. H., Riffeser, A., Kudritzki, R.-P., Matthias, M., Freeman, K. C., Arnaboldi, M., Capaccioli, M., & Gerhard, O. E. 2001, ApJ, 563, 135
Merrett, H. R., Kuijken, K., Merrifield, M. R., et al. 2003, MNRAS, 346, L62
Merrett, H. R., Merrifield, M. R., Douglas, N. G., et al. 2006, MNRAS, 369, 120
Meyssonnier, N., Lequeux, J., & Azzopardi, M. 1993, A&AS, 102, 251
Mihos, J. C., Janowiecki, S., Feldmeier, J. J., Harding, P., & Morrison, H. 2009, ApJ, 698, 1879
Nolthenius, R., & Ford, H. C. 1987, ApJ, 317, 62
Peng, E., Ford, H., & Freeman, K. 2004, ApJ, 602, 685
Skrutskie, M. F., et al. 2006, AJ, 131, 1163
Su, D. Q., Cui, X., Wang, Y., & Yao, Z. 1998, Proc. SPIE, 3352, 76
Theuns, T., & Warren, S. J. 1997, MNRAS, 284, L11
Walterbos, R. A. M., & Kennicutt, R. C., Jr. 1987, A&AS, 69, 311
Wang, S.-G., Su, D.-Q., Chu, Y.-Q., Cui, X., & Wang, Y.-N. 1996, Appl. Opt., 35, 5155
Xing, X., Zhai, C., Du, H., Li, W., Hu, H., Wang, R., & Shi, D. 1998, Proc. SPIE, 3352, 839
York, D. G., et al. 2000, AJ, 120, 1579
Zhao, Y. 2000, Proc. SPIE, 4010, 290
Zhu, Y., Hu, Z., Zhang, Q., Wang, L., & Wang, J. 2006, Proc. SPIE, 6269, 20